Estimation of Dye Configuration from Conventional Chiroptical Spectra of Porphyrin Integrates: Combination of Exciton Theory with Monte Carlo Molecular Structural Simulation

Takeshi Yamamura,* Takaharu Mori, Yoshiki Tsuda, Tomotaka Taguchi, and Norikazu Josha

Department of Chemistry, Faculty of Science, Tokyo University of Science, Kagurazaka, Shinjuku-ku, Tokyo 162-8601, Japan

Received: August 8, 2006; In Final Form: November 4, 2006

Dye integrates (arrays and aggregates) are the subject of current interest in photochemical devices. However, they are in general not suitable for X-ray crystallography because of their poor crystallinity. Here, we improved a simple method of estimating dye configurations in porphyrin integrates from their visible absorption (AB) and circular dichroism (CD) spectra. For this purpose, we calculate the dipolar and optical rotatory strengths of an integrate on the basis of the exciton theory for a given porphyrin configuration, generate the theoretical AB and CD spectra of the dye integrate using a phenomenological line shape function, a Voigt function with an adjustable line width, and optimize the configuration by minimizing the square sum (*S*) of the difference between the observed and calculated spectra. We adopted two optimization methods to achieve a least-squares fit between the calculated and observed spectra: the Metropolis Monte Carlo (MC) method, which incorporates *S* into the molecular force-field energy as a constraint, and the quasi-Newton (QN) method, which numerically minimizes *S* and uses no molecular force field. To check the feasibility of these methods, we simulated the AB and CD spectra of Tröger's base and meso−meso-linked porphyrins using the QN program, then compared the dye configurations with their X-ray structures. The calculated dye configuration of Tröger's base porphyrin is sufficiently in agreement with that of the X-ray structure (RMSD = 0.21 Å for the ZnS_4 center), whereas that of meso−meso-linked porphyrin was not. These results were discussed in terms of charge transfer between two porphyrins. Finally, we applied the QN and MC methods to the structural estimation of a newly prepared peptide-linked bis(porphyrin) Boc−$(Por^{Zn,S})_2$−OBu^t. The best configurations estimated by these two methods were sufficiently in agreement with each other.

1. Introduction

Covalently or noncovalently bound dye integrates (arrays and aggregates) are important in biology, chemistry, and materials science. Photosynthetic organs use chlorophyll integrates not only for energy transfer in light-harvesting complexes[1] but also for photoinduced charge separation in reaction centers.[2] The effectiveness of such processes in nature has extensively stimulated physicochemists[3−4] and synthetic chemists.[5−6] On the other hand, the industry uses dye integrates for liquid crystals,[7] dye-sensitized solar cells,[8] and photographic sensitizers.[9] Their applications in nonlinear optics and to multiphoton absorption are also the objects of current research in photophysics and photochemistry.[10]

Porphyrin is one of the most familiar dyes in photochemistry. Much work has been carried out to synthesize covalently connected porphyrin arrays. However, most arrays have poor crystallinity. Hence, it is difficult to subject them to X-ray crystallography except for well-designed cases.[11] Nuclear magnetic resonance (NMR) spectroscopy[12] and powder X-ray diffraction (XRD) analysis[13] may also be available for obtaining structural information; however, they have experimental limitations such as line broadening and crystallinity, respectively. Consequently, for most porphyrin integrates, particularly aperiodic porphyrin integrates, there is no choice but to rely on conventional spectroscopies (e.g., visible absorption (AB) and circular dichroism (CD) spectroscopies), at least, at the start of the structural discussion.[14] Such discussions remain at the qualitative stage in terms of porphyrin configuration. On the other hand, molecular mechanics (MM)[15] and molecular dynamics (MD)[16−17] calculations are frequently used in discussing porphyrin configurations in integrates, to which excitonic[18] and molecular orbital (MO) calculations[19−25] are appended to discuss whether the configurations reproduce the observed AB and CD spectra.[17,26] However, the computations that have thus far been reported contain no reliable feedback mechanism from observed spectra.

In this study, we introduced a simple feedback method of carrying out least-squares fitting between configuration-dependent theoretical and observed spectra into the computation. We adopted two optimization methods different in structural search: the quasi-Newton (QN) method and the Metropolis[27] Monte Carlo (MC) method. We provide the details of these calculations and results of the feasibility check for two chirogenic compounds, namely, Tröger's base porphyrin (Figure 1a)[28] and meso−meso-linked bis(porphyrin) (Figure 1b),[29] as well as results of the application of these two calculation methods to the structural analysis of a new bis(porphyrin), Boc−$(Por^{Zn,S})_2$−OBu^t (Figure 1c),[30] that was synthesized by condensing two unnatural amino acids $Por^{Zn,S}$. Porphyrin configurations yielded by the two methods are well superimposed. We also discuss the characteristics of the QN and MC methods.

* Corresponding author. E-mail: tyamamur@rs.kagu.tus.ac.jp.

10.1021/jp065111k CCC: $37.00
Published on Web 02/24/2007

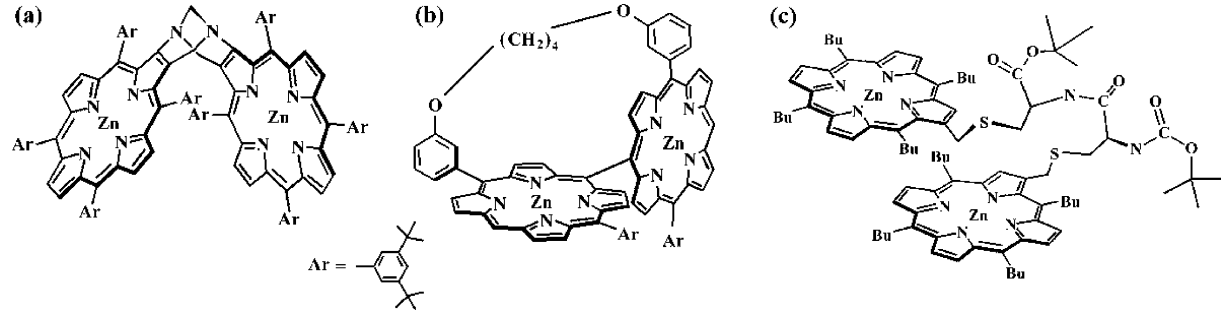

Figure 1. (a) Tröger's base porphyrin synthesized by Crossley et al.[28] (b) Meso−meso-linked bis(porphyrin) synthesized by Yoshida et al.[29] (c) New porphyrin dimer linked by peptide bond.[30]

2. Methods

There are many approaches to calculating configuration-based AB and CD spectra for dye integrates. They differ in the treatment of the interaction among excited and ground-state dyes, as well as in the introduction of spectral functions. For example, one approach assumes dipolar interactions among electronic oscillators and uses Kronig−Kramers transform relations for the direct calculation of the spectra.[31] The MO method enables the calculation of interactions among point monopoles to obtain the AB and CD line spectra[32] in conjunction with the quantum theory of CD[33] and the dipole velocity method.[34] It also yields ab initio line shape functions[22−24] by taking the Franck−Condon factor, vibration statistics, and vibronic interactions into account.[35−37] On the other hand, the exciton method adopts dipole approximation. Because of its simplicity, this method is most frequently used to calculate the positions and strengths of AB and CD spectra of small and aperiodic dye integrates in solution.[38] Systematic analyses of covalently connected dye systems were carried out by the exciton chirality method by the groups of Nakanishi, Berova, and Woody.[17,26] The exciton method has also been applied to the periodic and aperiodic chlorophyll systems in photosynthetic organs to analyze their dynamical behavior.[35−39]

Among the above-mentioned approaches, we chose the exciton method as the simplest for the calculation of electronic state, and replaced all other interactions by the phenomenological line shape function, i.e., the Voigt function.[40] This is because the least-squares fitting requires multiple steps: structure-based electronic state calculations, dipolar and optical rotatory strength calculations, spectral-line-shape calculations, and optimizations. Thus, we need to choose a fast method of computing the electronic states and spectral line shapes to save computing time.

In the fitting, we minimized the square sum (S) defined by

$$S = \alpha\sum_{\lambda}(f(\sigma)_{\lambda}^{\mathrm{obs}} - f(\sigma)_{\lambda}^{\mathrm{calc}})_{\mathrm{AB}}{}^{2} + \beta\sum_{\lambda}(f(\sigma)_{\lambda}^{\mathrm{obs}} - f(\sigma)_{\lambda}^{\mathrm{calc}})_{\mathrm{CD}}{}^{2} \quad (1)$$

where the superscripts "obs" and "calc" indicate the observed and calculated spectra, respectively. Details of the familiar exciton calculation and the choice of the line shape function are given in the Appendices. α and β are constants that regulate the contributions of AB (ϵ) and CD ($\Delta\epsilon$) spectra, respectively.

We adopted two optimization methods different in structural search: the quasi-Newton (QN) method and the Metropolis[41] Monte Carlo (MC) method. The QN method generates random sets of porphyrin configurations and directly optimizes S by the quasi-Newton method by varying the relative orientation. The MC method incorporates S into the molecular-force-field energy as a constraint and minimizes the total energy. This method is an MC analogue of the restrained molecular dynamics (MD) calculations that are frequently used in NMR and X-ray structural analyses.[42]

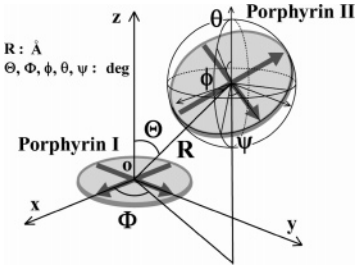

Figure 2. Definition of mutual configuration of two porphyrins: polar coordinates (R, Θ, Φ) and Euler angles (ϕ, θ, ψ).

Parameters, Variables, and Optimization. For the optimization of AB and CD spectra of dye integrates, we need to determine the strengths of the transition dipoles μ_{px} and μ_{qy} (eq 5 in Appendix) instead of those obtained from the monomer in solution[8,17] because the dipole strength of a porphyrin in dye integrates is smaller than that of the monomer in solution owing to hypochromism.[43] Although Stark spectroscopy is effective for measuring the dipole moment shift $\Delta\mu$,[44] this method is not commonly used. Thus, in common cases, the transition dipoles are determined by the spectral simulation. We also need the true transition energies E_x and E_y to solve eq 4 in Appendix; however, it is difficult to determine the true E_x and E_y of a monomer in integrates because dyes electronically interact with others in integrates. Therefore, we treated E_x and E_y as variables. We also adopted variable line widths ($\Delta\sigma_i$; see eqs 8−10 in the Appendix) instead of fixed ones by referring to dynamical exciton calculations for reaction centers[35−37] and antenna chlorophylls,[38−39] as well as explicit potential surface calculations for excitons in dimers.[45−46] α and β in eq 1 are determined so as to reproduce the structures of standard compounds because they depend on the type of target compound (for porphyrins, ϵ is generally on the order of 10^5, whereas $\Delta\epsilon$ is on the order of $10-10^3$), as well as the method used (the QN or MC method).

Quasi-Newton Method. In this method, the configuration of a pair of porphyrins is given by a set of six variables, R, Θ, Φ, ϕ, θ, and ψ. Of these variables, R, Θ, and Φ represent the polar coordinates of the central metal ion of the second porphyrin; on the other hand, ϕ, θ, and ψ represent the Euler angles that define the relative rotation of the second porphyrin to the first porphyrin (Figure 2). At the starting point of the minimization, the six variables are randomly generated, and the corresponding spectra are calculated; then, the coordinates are varied to minimize S. To avoid the local-minima problem, 20000 starting coordinates are generated. However, structures optimized by this method often suffer from steric hindrance. Therefore, we incorporated a subroutine into the program to discard such cases.

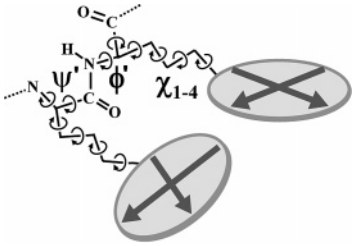

Figure 3. Porphyrin conformation given by dihedral angles (ϕ', ψ', χ^{1-4}). The Cartesian coordinates of all atoms were calculated from the internal coordinates using the GENER subroutine included in ECEPP.[53−54]

Monte Carlo Method. This method was developed to search for energetically rational structures. For this purpose, we combined S with AMBER force field (version 6)[47−48] as a constraint, as given by eq 2,

$$E_{\text{total}} = \sum_{\text{dihedrals}} \frac{V_n}{2}[1 + \cos(n\eta - \gamma)] + \sum_{i<j}\left[\frac{A_{ij}}{R_{ij}^{12}} - \frac{B_{ij}}{R_{ij}^{6}}\right] + \sum_{i<j}\frac{q_i q_j}{\epsilon R_{ij}} + S \quad (2)$$

and minimized total energy by the Metropolis MC method (see references and notes[52] for the definition of the variables). In the MC calculation, we adopted the dihedral angles ϕ' and ψ' for the peptide main chain[52,53] and χ_{1-4} for the side chains as variables (Figure 3) instead of Cartesian coordinates, and fixed other inner coordinates, such as bond lengths and angles, to save computation time. For this purpose, we applied the GENER subroutine of ECEPP developed by Momany et al.,[54] in which we modified the residue data so as to reproduce the energies and structures by AMBER calculation for several standard residues.[55] This program can simulate peptide arrays with up to 99 porphyrins.

Applicability Check of Exciton Program. To check the applicability of the exciton part, we used the QN program,[56] because the QN method is not biased against the molecular force field. In this check, we simulated the AB and CD spectra of two compounds: Tröger's base porphyrin synthesized by Crossley et al.[28,57] and the meso−meso-linked porphyrin synthesized by Yoshida et al.[29] These are the only two small compounds for which AB and CD spectra, as well as X-ray crystallography data, are available among many porphyrin integrates. The availability of the CD spectrum in addition to the AB spectrum increases the reliability of spectral simulation in comparison with the use of the AB spectrum only.

In the calculation, R was varied from 6 to 9 Å and Θ, Φ, ϕ, θ, and ψ were varied from −90 to +90°. The transition dipole moment $\mu_x = \mu_y$= 8.06 D and excitation energy $E_x = E_y$ = 23 320 cm^{-1} were found to best reproduce the spectra of Tröger's base porphyrin. $E_x = E_y$ was determined from the search in the range 23200−23700 cm^{-1}. The dipole moment and excitation energy taken from the Soret band spectrum of [5,10,15,20-tetrakis(3,5-di-*tert*-butylphenyl)porphyrinato]zinc-(II) did not reproduce the spectra, although this compound is the monomer that most closely resembles to Tröger's base porphyrin and has no skeletal distortion arising from repulsive forces among meso-aryl groups. $\alpha = 1.0$ and $\beta = 1.0 \times 10^5$ gave the most reliable results for this case. The conditions for the simulations of Tröger's base porphyrin and the meso−meso-linked porphyrin are summarized in Table 1.

Plotted in Figure 4 are log(S) vs (R, Θ), log(S) vs (R, θ), and log(S) vs (Θ, θ) for Tröger's base porphyrin. From these three plots, it is possible to know that (R, Θ, θ) converges to (8.2, ±42, ±56).

However, the convergence of log(S) for (ϕ, θ, ψ) was not unequivocal. This means that the spectra are predominantly dependent on (R, Θ, θ); therefore, we carried out a second search by fixing (R, Θ, θ) at (8.2, ±42, ±56). This search yielded log(S) = 10.29 for (Φ, ϕ, ψ) = (−59, −66, 26) as the optimum result. The calculated spectra and porphyrin configuration are respectively shown in Figures 5 and 6 together with the X-ray structure. As demonstrated in these figures, the simulation successfully reproduced the X-ray configuration (the RMSD of the ZnN_4 center was 0.21 Å) with good refinement parameters, R_{AB} and R_{CD} (see the figure caption). Considering the structural change from the solid to the solution state, as well as the difference in the central metal ion,[58] the small deviation seen here can be ignored. The parameters for the spectra of Tröger's base porphyrin are summarized in Table 2.

The search for the meso−meso-linked bis(porphyrin) (the conditions for the calculation are listed in Table 1) converged to (R, Θ, θ) = (6.8, ±80, ±62). (Φ, ϕ, ψ) seemed to converge to (−66, −44, 81) although this result was not conclusive unlike the result of Tröger's base porphyrin. The results are summarized in Table 2 and Figures 7 and 8. As seen in Figure 7, the calculated structure seems to reproduce the AB spectrum of this bis(porphyrin); however, the two porphyrins are abnormally close to each other at the meso−meso bond and the bond vector is not in plane, as shown in Figure 8 (RMSD = 0.95 Å for the ZnN_4 core).

Application of MC Method to Analysis of Peptide-Linked Porphyrin Dimer. We then combined the exciton subroutine with an MC subroutine, and applied this newly written program to the analysis of a new compound, Boc−(Por^{Zn,S})$_2$−OBu^t (see Figure 1c).[30] This compound showed a strong blue shift in its Soret-band region in CH_2Cl_2, a high-field shift in the β-pyrrole region of the ^{1}H−NMR spectrum in CD_2Cl_2, and a low fluorescence yield. From this experimental evidence, the compound was expected to have a face-to-face-like dye configuration.

The dipole moment $\mu_{x,y}$ = 7.28 D^2 and Soret-band energy $E_{x,y}$ = 23 610 cm^{-1} were determined by the QN and MC simulations of the AB and CD spectra of Boc−(Por^{Zn,S})$_2$−OMe as described in the section of parameters, variables, and

TABLE 1: Conditions of Quasi-Newton Calculations for Spectral Optimization of Tröger's Base Porphyrin,[28] Meso−Meso-Linked Porphyrin,[29] and Boc−(Por^{Zn,S})$_2$−OBu^t [30]

	Tröger's base	meso−meso linked	Boc−(Por^{Zn,S})$_2$−OBu^t
initial structure	20 000	20 000	20 000
R (Å)	7−9	7−9	6−7
Θ, Φ, ϕ, θ, and ψ (deg)	−90 to +90	−90 to +90	−90 to +90
E_x, E_y (cm^{-1})	23320	24387	23610
$\mu_{x,y}$ (D^2)	65	70	53
α	1.0	1.0	1.2×10^{-8} [a]
β	5.0×10^4	1.0×10^4	0.033[a]

[a] The weighting factors for Boc−(Por^{Zn,S})$_2$−OBu^t were adjusted to those of the MC calculations to enable comparison.

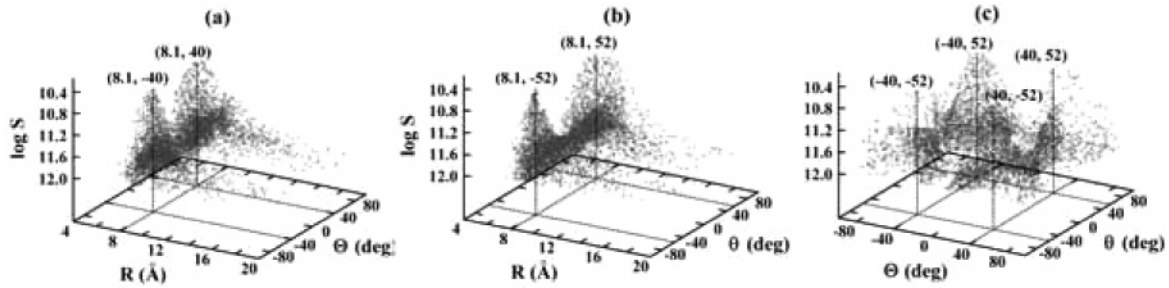

Figure 4. Plots of log S vs (a) $R-\Theta$, (b) $R-\theta$, and (c) $\Theta-\theta$. (R, Θ, θ) giving the lowest log(S) distribution around (8.1, ±40, ±52).

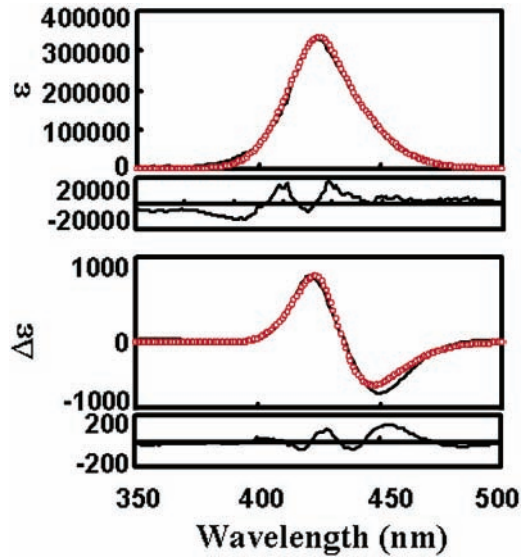

Figure 5. Comparison of optimized and observed AB (upper) and CD spectra (lower) of Tröger's base porphyrin. The experimental data (in $CHCl_3$) measured by Crossley et al.[28] are shown by solid lines. The results of optimization are shown by red circles. Differential spectra between the calculated and observed ones are shown below the AB and CD spectra. Refinement parameters R_{AB} and R_{CD} for AB and CD spectra (see Appendix) are 0.0671 and 0.174, respectively.

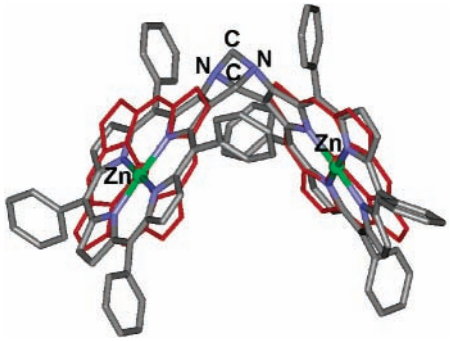

Figure 6. Optimized structure (red line) of Tröger's base porphyrin compared with that of X-ray crystallography (color by element; CSD code, YUKFEP). RMSD for the MN4 core was 0.21 Å. *tert*-Butyl groups on the phenyl rings are not shown for clarity.

optimization. Ten MC processes were carried out for different seed values starting from a pleated structure, under the following conditions: 5×10^5 steps for each process, $\Delta\phi'$ and $\Delta\psi' = 8°$ for each step, annealing from 2000 to 300 K, and no cutoff for Coulomb and van der Waals interactions. The weighting factors for AB and CD terms were set at $\alpha = 1.2 \times 10^{-8}$ and $\beta = 0.033$ to fit the energies of molecular force fields.

The optimized AB and CD spectra of Boc−$(Por^{Zn,S})_2$−OMe which gave the lowest log(S) and E_{AMBER} (≈ −138 kcal/mol) are shown in Figure 9 with the experimental spectra (the adoptability was 16%). The molecular structure is shown in Figure 10.[59] Note that these spectra and the structure are those averaged for the final 1000 steps after minimization. The optimized MC structure has four combinations of (Θ, Φ, ϕ, θ, ψ) due to symmetry. We listed all the (R, Θ, Φ, ϕ, θ, ψ) sets in the MC simulation in Table 3 to enable comparison with those in the QN simulation described below. The excitation energies (E), dipole strengths (D), optical-rotatory strengths (R), and half-widths ($\Delta\sigma$) of the bands obtained by MC calculations are summarized in Table 4.

The QN calculations for the same compound (conditions are listed in Table 1) were optimized at (R, Θ, θ) ≅ (6.5, ±33, 0, −60, 33, −36),[60] giving log(S) = 2.61. The excitation energies (E), dipole strengths (D), optical-rotatory strengths (R), and half-widths ($\Delta\sigma$)of the bands obtained by QN calculations are also listed in Table 4. The spectra and structure obtained by QN calculations are superimposed (by dotted lines) on those obtained by MC calculation in Figures 9 and 10, respectively, for comparison. Figure 10 shows that porphyrin configurations obtained by these two methods are in good agreement (RMSD = 0.28 Å for the ZnN_4 coordination unit) with each other, although their (Θ, Φ, ϕ, θ, ψ) sets differ from each other in appearance (Table 3). In these structures, two porphyrins are obliquely face-to-face with an almost parallel but not $\pi-\pi$-stacked configuration. The Zn−Zn distances of the two porphyrins were 6.56 and 6.49 Å for the MC and QN structures, respectively; on the other hand, the plane distances were the same (approximately 5.0 Å).

4. Discussion

Applicability. As described in the above section (see Figures 6 and 8), the QN calculation for Tröger's base porphyrin[28] reproduces well the X-ray configuration, as well as the AB and CD spectra, whereas the calculation for meso−meso-linked porphyrin[29] gives abnormal results. This result is due to the difference in porphyrin−porphyrin interaction mode between the two compounds. Two porphyrins of the Tröger's base are spatially separated and there is no direct bond or $\pi-\pi$ stack between the two porphyrins, whereas those in the meso−meso-linked are directly bound at the meso positions. The exciton theory is a simple approximation method based on a dipolar interaction; therefore, it does not correspond to cases in which strong electronic interactions among dyes exist. Such interactions distort the spectra from those predicted by the exciton theory. That is, the exciton method is not effective for dye integrates in which π-orbitals of porphyrins are in contact, as observed in several cases of J- and H-aggregates,[61−62] or porphyrins are linked by direct bonds, for which the mixing of charge transfer is pointed out.[29] Note that charge transfer also depends on the distance and orientation of the component π-orbitals of neighboring porphyrins. For such systems, it is necessary to develop a new random-move program on the basis of the MO theory. A preliminary MO/QN calculation for Tröger's base porphyrin

TABLE 2: Excitation Energies (E), Dipole Strengths (D), Optical Rotatory Strengths (R), and Line Widths ($\Delta\sigma$) of Calculated Spectra of Tröger's Base Porphyrin and Meso−Meso-Linked Porphyrin

	Tröger's base porphyrin				meso−meso-linked porphyrin			
band	E^i (cm^{-1})	D^i (D^2)	R^i (DBM^a)	$\Delta\sigma^i$ (cm^{-1})	E^i (cm^{-1})	D^i (D^2)	R^i (DBM^a)	$\Delta\sigma^i$ (cm^{-1})
1	24080.4	81.9	4.9	1300	26504.6	8.9	−1.8	2500
2	23522.0	110.3	16.9	900	24879.2	97.2	26.4	2000
3	23109.9	18.9	−16.6	1700	23894.8	43.3	−25.4	650
4	22551.6	47.3	−4.6	1050	22269.4	131.5	1.5	1650

[a] Debye-Bohr magneton.

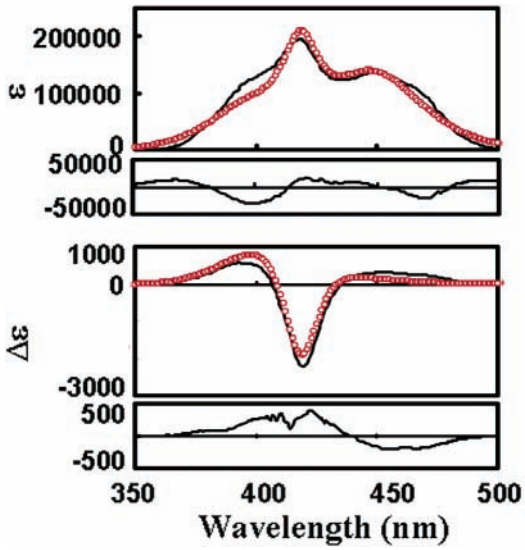

Figure 7. Comparison of optimized and observed AB (upper) and CD (lower) spectra for meso−meso-linked porphyrin. The experimental data (in CH_2Cl_2) measured by Yoshida et al.[29] are shown by black solid lines. The results of optimization are shown by red circles. Differential spectra between the calculated and observed ones are shown below the AB and CD spectra. Refinement parameters R_{AB} and R_{CD} (see Appendix) were 0.131 and 0.106 for AB and CD spectra, respectively.

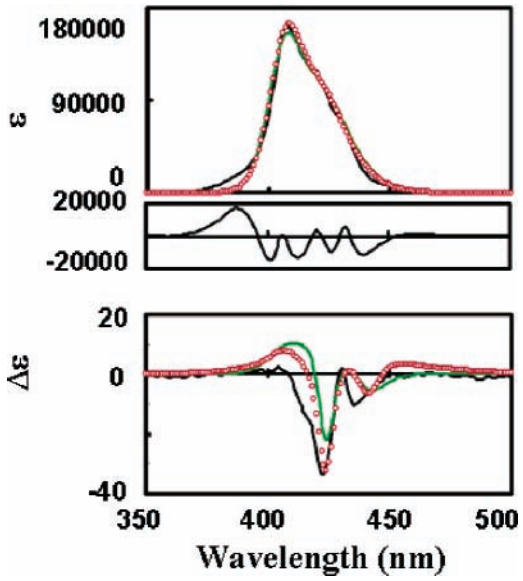

Figure 9. AB (upper) and CD (lower) spectra of Boc−(Por^{Zn,S})$_2$−OMe. Black solid lines: experimental data (in CH_2Cl_2). Red circles: Monte Carlo (MC) method. Green solid lines: Quasi-Newton (QN) method. Only the differential AB spectrum is shown here (below the AB spectra). Refinement parameters of the AB spectra R_{AB} (see Appendix) optimized by MC and QN methods were 0.104 and 0.107, respectively.

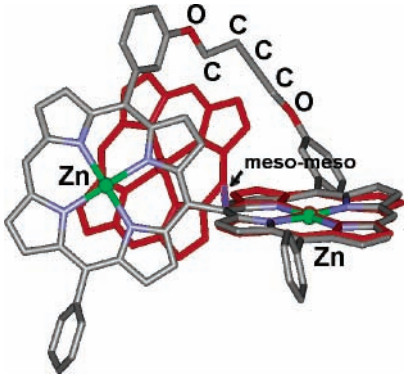

Figure 8. Optimized structure (red line) of meso−meso-linked porphyrin compared with that of X-ray crystallography (color by element; CSD code, HUQHAC). RMSD for the MN_4 core was 0.95 Å. *tert*-Butyl groups on the phenyl rings are not shown for clarity.

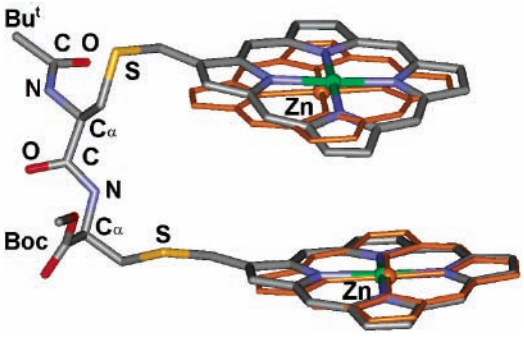

Figure 10. Structures of TBP dimer calculated by Monte Carlo method (color by element) and quasi-Newton (QN) method (orange line). RMSD for ZnN_4 core between the two structures was 0.28 Å.

using a new program, which was written on the Warshel and Alden algorithms[22−24] that incorporate the effect of charge transfer arising from $P_\pi-P_\pi$ interactions, indicated that our exciton program has the same accuracy as the MO method as long as we calculate systems in which porphyrins are spatially separated. The exact point where the dipole approximation breaks down would be clarified by the systematic use of such MO methods on the whole space of (R, Θ, Φ, ϕ, θ, ψ).

The evaluation of the methods described here should be carried out for sufficient number of standards that provide AB and CD spectra, as well as the results of X-ray crystallography, and that they are different in R, Θ, Φ, ϕ, θ, and ψ; however, we could not find any other examples than the two compounds discussed above from the viewpoint that the integration numbers of porphyrins are within the effective range of our method.

Finally, our method is not applicable to the solution that is largely contaminated with conformers. In comparison with the simulation of the AB spectrum of Boc−(Por^{Zn,S})$_2$−OMe, the optimization of its CD spectrum is not sufficient and gave fairly large residues in both MC and QN methods. This is explained by the existence of a conformational isomer in the solution. We found that the solution of Boc−(Por^{Zn,S})$_2$−OMe is an equilibrium mixture of two conformers: major and minor species. The AB spectrum of the minor species was similar to the major

TABLE 3: Polar Coordinates and Euler Angles for Boc−(Por^{Zn,S})$_2$−OMe Obtained by the Monte Carlo (MC) and Quasi-Newton (QN) Methods

		R (Å)	Θ (deg)	Φ (deg)	ϕ (deg)	θ (deg)	φ (deg)
MC	1	6.56	40.7	158.7	61.3	11.4	293.4
	2	6.56	40.7	158.7	241.3	348.6	113.4
	3	6.56	319.3	338.7	61.3	11.4	293.4
	4	6.56	319.3	338.7	241.3	348.6	113.4
quasi-Newton		6.49	±33.0	−60.0	3.0	0	−3.0

species just after the HPLC isolation, but the CD spectrum was different. Our calculation indicated that these two are the mirror images in the peptide-chain folding (Supporting Information).

Accuracy, Sensitivity, and Uniqueness. In the case of a small $V_{px:qy}$ (large R or $\theta \cong 0$ and $3\cos^2\Theta - 1 \cong 0$), the dye configuration is nearly achiral and the energy separation among the exciton states is small. In such cases, deconvolution becomes dominated by experimental noise and deconvolution error. Moreover, the sensitivity of the search becomes poor. Therefore, the accuracy of the spectral simulation of dye arrays in solution depends not only on the Davidov splitting but also on the line shape function we adopt, as well as experimental and simulation accuracy. The accuracy will be a complicated function of ΔE^i (the separation of E^i), $\Delta\sigma_i$, $D^i/\Delta\sigma_i$, and $R^i/\Delta\sigma_i$,[64] the noise and off-set levels of the spectra, the wavelength error, and refinement parameters given by eqs 11a and 11b (see Appendix). The step width of the search should be added to this list in case of the MC method. Therefore, it is impossible to give an equation that quantitatively evaluates the accuracy of the simulation, that is to say, the limit of the simulation. Instead, we empirically evaluated the limit for a porphyrin dimer by changing R, Θ, Φ, ϕ, θ, and ψ. This survey clarified that the methods we developed here reproduces the spectra and original structures of the cases where ΔE^i is larger than ~200 cm^{-1} (we assumed that the spectra include ±0.5 nm of wavelength inaccuracy). Rapid decrease of the adoptability of structure was observed between 100 and 50 cm^{-1}; however, it must be noted that the adoptability was dependent on the mutual orientation of the two porphyrins.

For the simulation of a dimer, the total number of variables is 12: μ, E, R, Θ, Φ, ϕ, θ, ψ, σ_i (i = 1, 2, 3, and 4); on the other hand, the number of parameters that are to be determined by simulation is also 12: E^i, D^i, and R^i ($i = 1 - 4$). Therefore, theoretically, it is possible to uniquely determine the porphyrin configuration of a dimer from the spectra. However, this is not guaranteed from a practical viewpoint even if our program achieves the best result within the framework of the exciton theory. For example, there may be a trajectory on which the dimer gives an approximately equal S in the phase space of (R, Θ, Φ, ϕ, θ, ψ). In other word, there may be a valley with a gentle slope around the true configuration in the landscape for given AB and CD spectra. Therefore, we carried out a whole-space survey for the spectra of Tröger's base porphyrin and Boc−(Por^{Zn,S})$_2$−OMe. In this survey, we clarified that the spectra of Tröger's base porphyrin only affords the configuration in Figure 6. On the other hand, the spectra of Boc−(Por^{Zn,S})$_2$−OMe gave a second configuration that is slightly higher in S than that shown in Figure 10. However, this configuration contained a van der Waals contact.

Spectrum Line Shapes, Line Widths, and Zero Cross Point. The zero cross point of the CD spectrum of Tröger's base porphyrin is shifted 12 nm toward the positive side from its absorption maximum (Figure 9). This is similar to those observed for the FMO protein and LH2 in appearance.[65] Theoretically, the zero cross point of a CD spectrum is in agreement with the corresponding absorption maximum as long as we assume a single line width for all exciton bands. In fact, Pescitelli et al.'s calculation for Tröger's base porphyrin[17] using the Lorentzian line shape showed a deviation between the zero cross points of the calculated and experimental CD spectra. In our pretrial on Tröger's base porphyrin, we also found that all calculations assuming Lorentzian, Gaussian, and Voigt functions as spectral line shapes could not remove the zero cross deviation as long as we assumed an equivalent line width for all exciton bands, in contrast to the fact that we reproduced the absorption band. Therefore, we assumed in this study variable line widths for different exciton bands and adopted a simple Voigt function (eq 8). The introduction of variable line widths conserving dipolar and optical-rotatory strengths markedly improved the simulation quality for Tröger's base porphyrin and almost completely removed the zero-cross-point deviation.[66] Note that both the X-ray structure and the MD structure of Tröger's base porphyrin calculated by using AMBER 6 in $CHCl_3$[67] afforded sufficient AB and CD spectra so long as we used variable line width, whereas those of meso−meso-linked porphyrin did not.

Important factors in the spectrum simulation of dye integrates are the choice of line-shape functions and line widths. It is widely accepted that the intramolecular harmonic vibration that couples to electronic transitions gives rise to Gaussian line shapes at high temperatures. In the solution state, the fluctuations of the surrounding media that also couple to the electronic states of the dyes contribute to line width broadening. Thus, in conventional exciton calculations for synthetic dye integrates, the line widths of exciton bands are frequently fixed to be equal irrespective of exciton level and line-shape function (Gaussian, Lorentzian, or Voigt function), particularly of the values of the monomers.[17,26,38,68] However, the different couplings of vibrations to different exciton levels have been known for at least 40 years.[69] The optical properties of aggregates, such as the line width of absorption and fluorescence, absorption intensity, fluorescence yield, and lifetime, depend on dye configuration and the number of dyes that are coherently coupled in the aggregates.[24,35−37,40,45] In recent calculations for chlorophyll systems in the crystalline states, different line widths have also been used for different exciton bands.[35−37,39,70−71] The homogeneous line width assumption may not be valid at least for the lowest excitonic level because this state may have a considerably longer lifetime than the other excitonic states at low temperatures.[39] According to the explicit and adiabatic treatment for an ideal homodimer,[45] the potential surfaces of exciton states depend on the electronic coupling between the monomers and the vibronic coupling in each monomer. A nonadiabatic expansion of this treatment to a heterodimer shows that the internal nuclear conformation of the molecules forming the dimer depends critically on the delocalization of the exciton state in the dimer and vice versa, and that the lower excitation state is localizing, whereas the upper one can be delocalizing in the subsequent time evolution by nuclear dynamics.[46]

Porphyrin planes are statically distorted in the solid state, and the excitation energies are dependent on such distortion.[72] MD calculations easily demonstrate that porphyrins dynamically distort. Such dynamical distortion of porphyrins brings about time-dependent changes in diagonal (E_i) and off-diagonal (V_{ij}) terms in eq 4 (see Appendix), which leads to an inhomogeneous line broadening,[73] the fluctuation in the energy gap between the component porphyrins, hence, the fluctuations in the upper and lower exciton potential surfaces, and a change in exciton delocalization length.[46,74−75] Consequently, the excitonic states of covalently connected dye array in solution[14,26,76]can have variable line widths.

TABLE 4: Excitation Energies (E), Dipole Strengths (D), Optical-Rotatory Strengths (R), and Half-Widths ($\Delta\sigma$) Obtained by MC and QN Simulations for Spectra of Boc−$(Por^{Zn,S})_2$−OMe

	MC simulation				quasi-Newton			
band	E^i (cm^{-1})	D^i (D^2)	R^i (DBM[a])	$\Delta\sigma^i$ (cm^{-1})	E^i (cm^{-1})	D^i (D^2)	R^i (DBM[a])	$\Delta\sigma^i$ (cm^{-1})
1	24551.1	105.9	0.139	700	24584.2	106.3	0.076	750
2	23632.1	105.5	0.275	1050	23640.7	106.2	0.149	1050
3	23587.9	0.772	−0.274	350	23579.3	0.089	−0.148	300
4	22668.9	0.324	−0.129	400	22635.8	0.003	−0.069	550

[a] Debye-Bohr magneton.

Effect of Constraint. Simple MD calculation for Tröger's base porphyrin reproduced the X-ray structure. This may indicate that the results of the MC calculation for this compound are not reflecting the spectral constraint. However, it should be noted that the QN method also afforded a similar configuration to the X-ray configuration; therefore, in this case, the constraint and force field synergetically operate to determine the structure. In practice, the structure of Boc−$(Por^{Zn,S})_2$−OMe obtained from the simple MD calculation could not reproduce the spectra.

Characteristics of the Quasi-Newton Method. The QN program we developed here took only 5 h to simulate the spectra of Tröger's base porphyrin starting from 20000 configurations using a desktop Linux PC equipped with a Pentium 4 chip (2.66 GHz). Structures obtained by the QN method are not biased against the molecular force field; however, it cannot calculate molecular structural insights other than the porphyrin orientation. In our preliminary calculations for Tröger's base porphyrin, we often found that one of the porphyrins invades the area of other porphyrins even in the calculations in which we achieved the best fit in spectra. Thus, in the program, we introduced a device for rejecting cases in which porphyrins are in van der Waals violation. However, we set the device that checks the van der Waals interaction to operate at $t > 0$, but not at the initial time $t = 0$. This is because, if the initial structure contains van der Waals contact, the calculation would immediately deviate from such a situation in the following steps, and may approach the optimized structure in a short time.

Although the algorithm can correspond to multiple porphyrin systems in principle, the number of independent porphyrins is practically limited to within three, as long as the Linux PC mentioned above is used; calculation time rapidly increases with the number of independent porphyrins. Consequently, the QN program is applicable to systems with up to 50 mers composed of a tandem repeat of two or three independent porphyrins written as $(A)_n$ and $(AB)_n$.

Although the program generates more than 20000 initial structures, the search is still crude for each variable. The larger we set the sampling number, the more the search becomes sufficient for obtaining a reliable structure; however, for the examples described in this paper, we found that a two-stage calculation is effective, in which we first determine the crude convergence in (R, Θ, θ) from a random survey, and then, by fixing (R, Θ, θ), we search the optimized point by surveying the (ϕ, θ, ψ) space. This is probably because two perpendicular transition dipoles of equivalent strengths, $\mu_x = \mu_y$, are used to describe porphyrin chromophores according to the four-orbital model.[63] This makes the convergence insensitive to the rotation of the second porphyrin. The two-stage calculation is probably unnecessary for dyes with single-transition dipoles. Consequently, we did not generalize the two-stage algorithm for all cases considering the merit of free sampling corresponding to targets. For example, it is possible to obtain the orientation angles of dyes in a Langmuir−Blodgett membrane by measuring polarized UV−vis spectra[14] and dye distance in a periodically stacked aggregate by X-ray diffraction analysis.[13] It is also possible to use the results of molecular dynamics and molecular orbital calculations. All information obtained by these methods provides an initial set of (R, Θ, Φ, ϕ, θ, ψ), and it is possible to carry out a weighted search around this initial set.

Characteristics of the MC Method. Our restrained MC method is an analogue of the restrained molecular dynamics.[42] In the course of our program development, we found that our calculations easily (after 500 steps) fall into local minima and the dye configuration does not change as long as we use a conventional MC process. This is explained as follows: small variations in dihedral angle bring about large displacements of porphyrin planes that lead to large changes in Davydov splitting, spectral line shape, and spectral intensity. This causes, in turn, a large deviation in S. The barrier caused by this deviation is too high to be overcome in the next step. In particular, changes in the line shape and strength of the CD spectrum are large in contrast to those of the AB spectrum. A move from a structure that gives good agreement in CD, but not in AB, between the calculated and observed spectra to another structure that shows good agreement in both spectra requires high activation energy for step out. This decreases the probability of structural change. To avoid this situation and solve the high-energy-barrier problem arising from CD spectral adjustment, we divided the process into two stages: (1) the first stage of 10000 steps without constraint and (2) the second stage of more than 10000 steps, where steps were divided into 200-step units with intermittent addition of constraint (Figure 11). Units with more than 200 steps were unnecessary because all minimizations with the spectral constraints fell into local minima within 200−5000 steps and stopped. The intermittent addition enabled the optimization to converge within 10 h (500 000 steps) for Boc−$(Por^{Zn,S})_2$−OMe. Step widths for dihedral angles ϕ' and ψ' were empirically determined to be 8°. The spectral change of CD was so sensitive that a step width larger than 10° prevented the convergence of the optimization, and a small step width of smaller than 3° did not change the molecular structure.

The time courses of the total energy (E_{total}), AMBER energy (E_{AMBER}), and constraint term (E_{AB+CD}) are shown in Figure 12, where only the means of the final 100 steps of the 1000-step repetitions in the second stage are plotted. On magnifying these E terms, we notice that E_{AMBER} rapidly increases at every 1000 steps then E_{AB+CD} lags behind the increase in E_{AMBER}. This indicates that van der Waals contact among the component atoms occurs just after the addition of the spectral term, and then the structural change that accumulated during the course of the relaxation causes large changes in spectra, particularly in the CD spectrum. The alternating prominences of E_{AMBER} and E_{AB+CD} indicate that the intermittent search algorithm operates satisfactorily without falling into a local minimum. The optimized structure is that giving the lowest E_{AMBER} (≈ -138 kcal/mol) + E_{AB+CD} (≈ -217 kcal/mol) at step 436 000 (shown in Figure 12a by a dashed arrow).

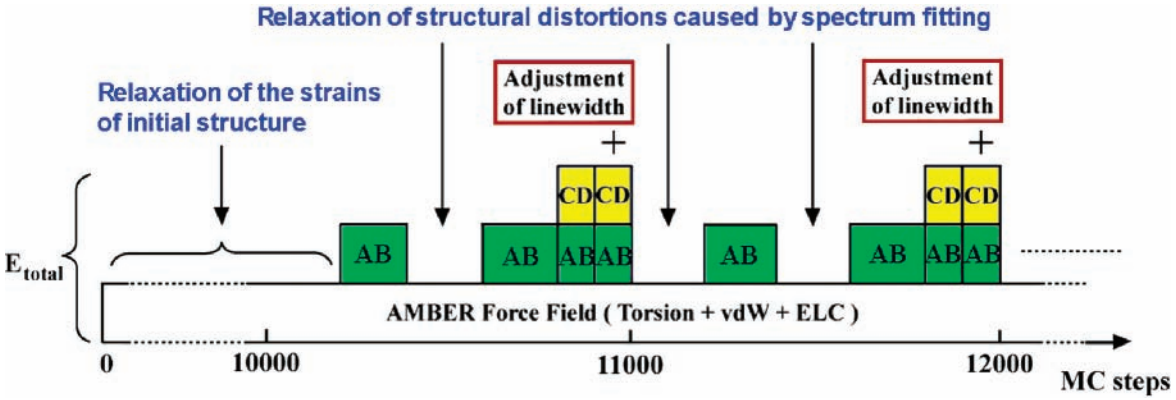

Figure 11. Constraint term, $\alpha\Sigma(f(\sigma)_{obs} - f(\sigma)_{calc})_{AB}^2) + \beta\Sigma(f(\sigma)_{obs} - f(\sigma)_{calc})_{CD}^2$, was intermittently added to the force field. In the first stage of the process (10000 steps), calculation was carried out only for AMBER energy ($\alpha = \beta = 0$) to remove the strain in the initial structure. In the second stage, steps were divided every 200 steps, where the AB (absorption) constraint was preferentially added for the initial 200 steps ($\alpha > 0$) and relaxed. After relaxation was achieved without constraint, the AB term was again added for 200 steps. In the next 100 steps, the constraint involving both AB and CD terms was added with and without changing line width. In the third stage, these processes between steps 10 000 and 11 000 were repeated until spectral optimization was achieved.

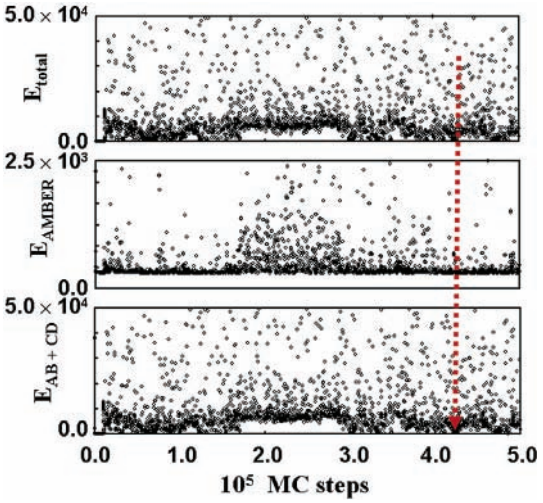

Figure 12. Time courses of the energies plotted for MC steps: (a) E_{total}; (b) E_{AMBER}, the AMBER force field term [torsion + van der Waals + electrostatic]; (c) spectral term, $[\alpha\Sigma(f(\sigma)_{obs} - f(\sigma)_{calc})_{AB}^2] + \beta\Sigma(f(\sigma)_{obs} - f(\sigma)_{calc})_{CD}^2]$. Conditions for MC calculations were as follows: number of starting structures, 10; starting structure, linear for main chain and random for side chain; step number, 500000; $\mu_{x,y}$, 53 D^2; weighting factor α, 1.2×10^{-8}; weighting factor β, 0.033; conditions of convergence, $E_{AMBER} < -135$ kcal/mol and $E_{UV+CD} < 350$ kcal/mol; dihedral angle step, 8°; temperature; annealed from 2000 to 300 K; electricity, distance dependent; cutoff, no; excitation energy of the monomer, 23610 cm^{-1}.

The MC method developed here has two characteristic points. (1) It adopts dihedral angles as variables, which enables a rapid descent along the slope of the energy landscape. (2) It allows us to escape from structural local minima with the help of an intermittently added spectral term; however, whether the search after the addition optimizes E_{total} depends on the molecular structure just before the addition. Therefore, it cannot always yield the optimized structure after one run. In practice, only three were obtained as optimized structures from 20 different seed values of random processes for Boc−$(Por^{Zn,S})_2$−OMe (adoptability 15%).

The MC program, at present, has only the force field parameters for porphyrin and the peptide main chain. Estimations for the other systems such as those containing cyanine dyes require molecular orbital calculations for new dyes and the registration of the results obtained. In addition, this program adopts dihedral angles (ϕ, ψ, χ) as variables for rapid calculation. Therefore, it is not applicable to systems other than peptides. An improvement in the program is now in progress to accommodate Cartesian-coordinate systems.

Finally, it should be pointed out that this method may suffer from bias error due to force field; that is, the obtained structure may be biased in spite of the existence of the spectral constraint.

Comparison of QN and MC Calculations. Although the QN and MC methods clearly reproduced the experimental AB spectrum of Boc−$(Por^{Zn,S})_2$−OBu^t, and the calculated spectra were similar to each other, the results were slightly different. The MC method reproduced the shoulder peak at 430 nm in the experimental AB spectrum, whereas the QN method did not. This result is explained as follows: (1) The intensity of the experimental CD spectrum of Boc−$(Por^{Zn,S})_2$−OBu^t is too small that the spectrum is contaminated by noise; therefore, the calculation could not allow an accurate fitting. (2) The actual molecule fluctuates in solutions; thus, calculations that take into consideration molecular fluctuation are necessary. In practice, the shoulder peak observed at 430 nm is not reproduced without assuming the mixing of more than two species. When the face-to-face configuration loses symmetry due to the mutual fluctuation of two porphyrins, a slight migration of the upper level to the lowest forbidden level is allowed, which leads to the generation of a 430 nm peak. Because the MC method averages many spectra in the time course, it automatically takes into account the effect of such molecular fluctuation. On the other hand, the stricter the converging condition of the QN method becomes, the more the calculation converges to a single structure, and the averaged structure loses the contamination by such asymmetric structures. This is the reason for the CD spectrum calculated by the MC method being more similar to the experimental one than to that calculated by the QN method (Figure 8).

Finally, the QN method is incompetent for the cases in which the simulation yields conformers from the experimental spectra, as discussed in the section of accuracy, sensitivity, and uniqueness. The MC method probably escapes from this problem with the help of its force field. Considering that the MC simulation takes a longer time than the QN method, the best way is to survey the candidates by the QN method, then to refine the best optimization by the MC method.

5. Summary

A new method based on the exciton theory was developed to estimate the dye configuration in porphyrin integrates from the simulation of their Soret-band AB and CD spectra. We

adopted Quasi-Newton and Monte Carlo methods to minimize the square sum (S) of the difference between the observed and calculated spectra, as well as the Voigt function for spectral line shape and variable line width. The MC method incorporates S into the molecular force field energy as a constraint to reproduce a chemically reliable structure. To check the feasibility of the exciton calculation in the QN and MC program, two bis(porphyrin)s were used as standards, for which Soret-band AB and circular dichroism spectra, as well as X-ray crystallography data, are available. This check confirmed that the methods yield good estimates of the experimental structures of porphyrin integrates as long as the component porphyrins are spatially separated. It is, however, ineffective for systems in which porphyrins are directly connected. Finally, these methods were applied to the structural estimation of a newly prepared porphyrin dimer linked by a peptide bond.

Acknowledgment. This work was supported by a Grant-in-Aid for Scientific Research on Priority Areas (417) from the Ministry of Education, Culture, Sports, Science and Technology (MEXT) of the Japanese Government.

Appendix

Equations Used for Calculations. To calculate porphyrin−porphyrin interacting systems, we followed the well-known form of the exciton method for porphyrin arrays, which is described by two vertical $\pi-\pi^*$ transition dipoles for each porphyrin based on Gouterman's four-orbital model.[63] The excited-state function Ψ of a porphyrin ensemble is approximated by the linear combination of $\phi_{s\alpha}$ ($s = 1-N$. $\alpha = x$ and y) given as

$$\Psi = C_{1x}\phi_{1x} + C_{1y}\phi_{1y} + C_{2x}\phi_{2x} + \cdots + C_{Nx}\phi_{Nx} + C_{Ny}\phi_{Ny} \quad (3)$$

In this equation, $\phi_{s\alpha}$ represents the state in which the sth porphyrin is excited, whereas all the other porphyrins are in the ground states. The energies of excited states are given by solving the secular equation

$$\begin{vmatrix} E_x - E & 0 & V_{2x:1x} & V_{2y:1x} & \cdots & V_{Nx:1x} & V_{Ny:1x} \\ 0 & E_y - E & V_{2x:1y} & V_{2y:1y} & \cdots & V_{Nx:1y} & V_{Ny:1y} \\ V_{1x:2x} & V_{1y:2x} & E_x - E & 0 & & \vdots & \vdots \\ V_{1x:2y} & V_{1y:2y} & 0 & E_y - E & & \vdots & \vdots \\ \vdots & \vdots & & & \ddots & \vdots & \vdots \\ V_{1x:Nx} & V_{1y:Nx} & & & & E_x - E & 0 \\ V_{1x:Ny} & V_{1y:Ny} & \cdots & \cdots & \cdots & 0 & E_y - E \end{vmatrix} = 0 , \quad (4)$$

where E_x and E_y are the x and y excitation energies of a monomer in the array, and $V_{px:qy}$ is the interaction between the dipoles of the pth and qth porphyrins, μ_x and μ_y respectively, given by

$$V_{px:qy} = \frac{\mu_{px}\mu_{qy}}{R_{pq}^{\ 3}} \{\mathbf{e}_{px}\cdot\mathbf{e}_{qy} - 3(\mathbf{e}_{px}\cdot\mathbf{e}_{pq})(\mathbf{e}_{qy}\mathbf{e}_{pq})\} \quad (5)$$

The dipole strength D_i of the ith exciton level is given by (7)[38]

$$D^i = \{\langle\Psi_0|\mu|\Psi^i\rangle\}^2 = \sum_{j=1}^{N} \{(C_{jx}^i)^2\mu_{jx}^{\ 2}\mathbf{e}_{jx}\cdot\mathbf{e}_{jx} + (C_{jy}^i)^2\mu_{jy}^{\ 2}\mathbf{e}_{jy}\cdot\mathbf{e}_{jy}\} + 2\sum_{k=1}^{N}\sum_{l>k}^{N} \{C_{kx}^i C_{lx}^i \mu_{kx}\mu_{lx}\mathbf{e}_{kx}\cdot\mathbf{e}_{lx} + C_{kx}^i C_{ly}^i \mu_{kx}\mu_{ly}\mathbf{e}_{kx}\cdot\mathbf{e}_{ly} + C_{ky}^i C_{lx}^i \mu_{ky}\mu_{lx}\mathbf{e}_{ky}\cdot\mathbf{e}_{lx} + C_{ky}^i C_{ly}^i \mu_{ky}\mu_{ly}\mathbf{e}_{ky}\cdot\mathbf{e}_{ly}\} \quad (6)$$

On the other hand, the optical rotatory strength R_i of the ith exciton level is given by (8).[38]

$$R^i = \mathrm{Im}\{\langle\Psi_0|\mu|\Psi^i\rangle\cdot\langle\Psi^i|\mathbf{M}|\Psi_0\rangle\} = -\pi\sigma_{0i}\sum_{j=1}^{N}\sum_{k>j}^{N} [R_{jk}\{C_{jx}^i C_{kx}^i \mu_{jx}\mu_{kx}(\mathbf{e}_{jx}\times\mathbf{e}_{kx})\cdot\mathbf{e}_{jk} + C_{jx}^i C_{ky}^i \mu_{jx}\mu_{ky}(\mathbf{e}_{jx}\times\mathbf{e}_{ky})\cdot\mathbf{e}_{jk} + C_{jy}^i C_{kx}^i \mu_{jx}\mu_{kx}(\mathbf{e}_{jy}\times\mathbf{e}_{kx})\cdot\mathbf{e}_{jk} + C_{jy}^i C_{ky}^i \mu_{jy}\mu_{ky}(\mathbf{e}_{jy}\times\mathbf{e}_{ky})\cdot\mathbf{e}_{jk}]\} \quad (7)$$

In eq 8, Ψ_0 is the wave function of the ground state, Ψ_i is the wave function of the ith state, μ is the electric-dipole operator, and $\mathbf{M}$ is the magnetic-dipole operator. σ_{0i} is the excitation energy from the ground state to the ith exciton level given in wavenumbers. C_{jx} is the binding constant of the wave function in eq 4, $\mathbf{e}_{j\alpha}$ represents the unit vector of $\mu_{j\alpha}$, and R_{jk} represents the distance between the central metal ions of the jth and kth porphyrins.

Spectral Function. Exciton and exciton chirality calculations give no information on line shapes. Therefore, as the line shape function, we introduced the Voigt function[40] given by

$$f(\sigma) = \sum_i \frac{\sigma_{0i}}{Kk_{\mathrm{V}}\Delta\sigma_i} I^i G^i(\sigma) L^i(\sigma) \quad (8)$$

$$G^i(\sigma) = \exp\left\{-\ln 2\,\frac{(\sigma-\sigma_{0i})^2}{k_{\mathrm{G}}\Delta\sigma_i^{\ 2}}\right\} \quad (9)$$

$$L^i(\sigma) = \frac{1}{1 + (\sigma-\sigma_{0i})^2/k_{\mathrm{L}}\Delta\sigma_i^{\ 2}} \quad (10)$$

where $f(\sigma)$ denotes the spectral function represented by ϵ (absorption coefficient) for AB spectra and that represented by $\Delta\epsilon$ (difference in absorption coefficient) or molar elipticity for CD spectra. I_{i} represents the dipolar strength D_i or optical rotatory strength R_i of the ith exciton state for AB and CD spectra, respectively. K is calculated as 9.184×10^{-39} cgs for AB spectra and 2.296×10^{-39} cgs for CD spectra. σ is the energy in wavenumbers. $2\Delta\sigma_i$(common to AB and CD spectra) is the half-height line width of the component Gaussian and Lorentzian line shapes for the ith exciton state. k_{V}, k_{G}, and k_{L} are coefficients that define the contributions of Voigt, Gaussian, and Lorentzian functions, respectively. We obtain $k_{\mathrm{V}} = 1.501882$ for $k_{\mathrm{G}} = k_{\mathrm{L}} = 1$.[77]

Refinement Parameters. Refinement parameters R_{AB} and R_{CD} for AB and CD spectra (see Appendix) are given by the next equations.

$$R_{\mathrm{AB}} = \frac{\sum_\lambda |\varepsilon_{\mathrm{calc}}^\lambda - \varepsilon_{\mathrm{obs}}^\lambda|_{\mathrm{AB}}}{\sum_\lambda (\varepsilon_{\mathrm{obs}}^\lambda)_{\mathrm{AB}}} \quad (11a)$$

$$R_{\mathrm{CD}} = \frac{\sum_\lambda |\varepsilon_{\mathrm{calc}}^\lambda - \varepsilon_{\mathrm{obs}}^\lambda|_{\mathrm{CD}}}{\sum_\lambda |\Delta\varepsilon_{\mathrm{obs}}^\lambda|_{\mathrm{CD}}} \quad (11a)$$

Supporting Information Available: Figures showing a flowchart of the quasi-Newton program, a flowchart of the Monte Carlo program, and the CD spectrum and the porphyrin

configuration of the minor conformer. This material is available free of charge via the Internet at http://pubs.acs.org.

References and Notes

(1) Fenna, R. E.; Matthews, B. W. *Nature* **1975**, *258*, 573−577. Li, Yi-Fen; Zhou, W.; Blankenship, R. E.; Allen, J. P. *J. Mol. Biol.* **1997**, *271*, 456−471. McDermott, G.; Prince, S. M.; Freer, A. A.; Hawthornthwaite-Lawless, A. M.; Papiz, M. Z.; Cogdell, R. J.; Isaacs, N. W. *Nature* **1995**, *374*, 517−521. Roszak, W.; Howard, T. D.; Southall, J.; Gardinar, A. T.; Law, C. J.; Isaaks, N. W.; Cogdell, R. J. *Science* **2003**, *302*, 1969−1972. Hofmann, E.; Wrench, P. M.; Sharples, F. P.; Hiller, R. G.; Welte, W.; Diederichs, K. *Science* **1996**, *272*, 1788−1791. Liu, Z.; Yan, H.; Wang, K.; Kuang, T.; Zhang, J.; Gui, L.; An, X.; Chang, W.; *Nature* **2004**, *428*, 287−292. Hino, T; Kanamori, E; Shen, J.-R; Kouyama, T. *Acta Crystallogr.* **2004**, *D60*, 803−809. Krauss, N.; Schubert, W. D.; Klukas, O;. Fromme, P.; Witt, H. T.; Saenger, W. *Nat. Struct. Biol.* **1996**, *3*, 965−973. Ferreira, K. N.; Iverson, T. M.; Maghlaoul, K.; Barber, J.; Iwata, S. *Science* **2004**, *303*, 1831−1838.

(2) Deisenhofer, J.; Epp, O.; Miki, K; Huber, K. R.; Michel, H. *Nature* **1985**, *318*, 618−624.

(3) Cinque, J.; Croce, R.; Holtzwarth, A.; Bassi, R. *Biophys. J.* **2000**, *79*, 1706−1717. Yang, M.; Damyanović; A.; Vaswani, H. M.; Fleming, G. R. *Biophy. J.* **2003**, *85*, 140−158. Byrdin, M.; Jordan, P.; Krauss, N.; Fromme, P.; Stehlik, D.; Schlodder, E. *Biophys. J.* **2002**, *83*, 433−457. Brixner, T.; Stenger, J.; Vaswani, H. M.; Cho, M-H.; Blankenship, R. E.; Fleming, G. *Nature* **2005**, *434*, 625−628. Frese, R. N.; Palacios, M. A.; Azzizi, A.; van Stokkum, I. H. M.; Kruip, J.; Rönger, M.; Karapetyan, N. V.; Schlodder, E.; van Grondelle, R.; Dekker, J. P. *Biochim. Biophys. Acta* **2002**, *1554*, 180−191. Zazbovich, V.; Matsuzaki, S.; Johnson, T. W.; Hayes, J. M.; Chitnis, P. R.; Small, G. *J. Chem. Phys.* **2002**, *275*, 47−59.

(4) Marcus, R. A. *Chem. Phys. Lett.* **1987**, *133*, 471−477. Bixon, M.; Jortner, J.; Michel-Beyerle, M. E.; Orgodnik, A. *Biochim. Biophys. Acta* **1989**, 977, 273−286. Kitzing, E.; Kuhn, H. *J. Phys. Chem.* **1990**, *94*, 1699−1702. Labahn, A.; Paddock, M. L.; McPerson, P. H.; Okamura, M. Y.; Feher, G. *J. Phys. Chem.* **1994**, *98*, 3417−3423. Heller, B. A.; Holten, D.; Kirmaier, C. *Science* **1995**, *269*, 940−945. Franzen, S.; Martin, J.-L. *Annu. Rev. Phys. Chem.* **1995**, *46*, 453−87. Hasegawa, J.; Nakatsuji, H. *J. Phys. Chem. B* **1998**, *102*, 10420−10430. Hasegawa, J; Nakatsuji, H. *Chem. Lett.* **2005**, *34*, 1242−1243.

(5) Osuka, A.; Nakajima, S.; Okada, T.; Taniguchi, S.; Nozaki, K.; Ohno, T.; Yamazaki, I.; Nishimura, Y.; Mataga, N. *Angew. Chem., Int. Ed.* **1996**, *35*, 92−95.

(6) Takahashi, R.; Kobuke, Y. *J. Am. Chem. Soc.* **2003**, *125*, 2372−2373. Peng, X.; Aratani, N.; Takagi, A.; Matsumoto, T.; Kawai, T.; Hwang, I.-W.; Ahn, T. K.; Kim, D.; Osuka, A. *J. Am. Chem. Soc.* **2004**, *126*, 4468−4469. Choi, M.-S.; Aida, T; Yamazaki, T.; Yamazaki, I. *Chem.*−*Eur. J.* **2002**, 8, 2667−2678. Yeow, E. K. L.; Ghiggino, K. P.; Leek, J. N. H.; Crossley, M. J.; Bosman, A. W.; Schenning, A. P. H. J.; Meijer, E. W. *J. Phys. Chem. B* **2000**, *104*, 2596−2606.

(7) Meredith, G. R.; VanDusen, J. G.; Williams, D. *J. Macromolecules* **1982**, *15*, 1385−1389. Wang, H.; Jin, M. Y.; Jarnagin, R. C.; Bunning, T. J.; Adams, W.; Cull, B.; Shi, Y.; Kumar, S.; Samulski, E. T. *Nature* **1996**, *384*, 244−247.

(8) O'Regan, B.; Grätzel, M. *Nature* **1991**, *353*, 737−740. Ehret, A.; Stuhl, L.; Spitler, M. T. *J. Phys. Chem. B* **2001**, *105*, 9960−9965.

(9) Collier, S. S. *Photogr. Sci. Eng.* **1974**, *18*, 430−440. Tani, T. *Photographic Sensitivity. Theory and Mechanisms*; Oxford University Press: New York and Oxford, U.K., 1995: 111−164.

(10) Dalton, L. R.; Harper, A. W.; Ghosn, R.; Steier, W. H;. Ziari, M.; Fetterman, H.; Shi, Y.; Mustacich, R. V.; Jen, A. K.-Y.; Shea, K. *J. Chem. Mater.* **1995**, *7*, 1060−1081. Ogawa, K.; Ohashi, A.; Kobuke, Y. *J. Am. Chem. Soc.* **2003**, *125*, 13356−13357.

(11) Balaban, T. S.; Goddard, R.; Linke-Schaetzel, M.; Lehn, J.-M. *J. Am. Chem. Soc.* **2003**, *125*, 4233−4239. Kano, K.; Fukuda, K.; Wakami, H.; Nishiyabu, R.; Pasternack, R. F. *J. Am. Chem. Soc.* **2000**, *122*, 7494−7502.

(12) Assfalg, M.; Banci, L.; Bertini, I.; Bruschi, M.; Giudici-Orticoni, M.; Turano, P. *Eur. J. Biochem.* **1999**, *266*, 634−643. Hofstra, U.; Koehorst, R. B. M.; Schaafsma, T. *J. Magn. Reson. Chem.* **1987**, *25*, 1069−1073. De Boer, I.; Matysik, J.; Amakawa, M.; Yagai, S.; Tamiaki, H.: Holzwarth, A. R.; De Groot, H. J. M. *J. Am. Chem. Soc.* **2003**, *125*, 13374−13375.

(13) Bhyrappa, P.; Wilson, S. R.; Suslick, K. S. *J. Am. Chem. Soc.* **1997**, *119*, 8492−8502. Diskin-Posner, Y.; Kumar, R. K.; Goldberg, I. *New J. Chem.* **1999**, *23*, 885−890.

(14) Liu, H.-Y.; Huang, J.-W.; Tian, X.; Jiao, X.-D.; Luo, G.-T.; Ji, L.-N. *Chem. Commun.* **1997**, 1575−1576. Purrello, R.; Bellacchio, E.; Gurrieri, S.; Lauceri, R.; Raudino, A.; Scolaro, L. M.; Santoro, A. M. *J. Phys. Chem. B* **1998**, *102*, 8852−8857. Arai, T.; Inudo, M.; Ishimatsu, T.; Akamatsu, C.; Tokusaki, Y.; Sasaki, T.; Nishino, N. *J. Org. Chem.*, **2003**, *68*, 5540−5549.

(15) Yatskou, M. M.; Koehorst, R. B. M.; Donker, H.; Schaafsma, T. J. *J. Phys. Chem. A* **2001**, *105*, 11425−11431. Ema, T.; Misawa, S.; Nemugaki, S.; Sakai, T.; Utaka, M. *Chem. Lett.* **1997**, *26*, 487−488.

(16) Bischoff, G.; Bischoff, R.; Hoffmann, S. *J. Porphyrins Phthalocyanines* **2001**, *5*, 691−701.

(17) Pescitelli, G.; Gabriel, S.; Wang, Y.; Fleischhauer, J.; Woody, R. W.; Berova, N. *J. Am. Chem. Soc.* **2003**, *125*, 7613−7628.

(18) Davydov, A. S. *Theory of Molecular Excitons*; McGraw-Hill: New York, 1962; pp 141−155. Davydov, A. S. *Theory of Molecular Excitons*; Plenum Press: New York and London, 1971; pp 23−112. Kasha, M.; Rawls, H. R.; El-Bayoumi, A. *Pure Appl. Chem.* **1965**, *11*, 371−392. Kasha, M. *Radiat. Res.* **1963**, *20*, 55−71. Pearlstein, R. M. *Excitons*; North-Holland Publishing Co.: Amsterdam, 1982; pp 735−770.

(19) Ohno, O.; Kaizu, Y.; Kobayashi, H. *J. Chem. Phys.* **1993**, *99*, 4128−4139.

(20) Hasegawa, J.; Ohkawa, K.; Nakatsuji, H. *J. Phys. Chem. B.* **1998**, *102*, 10410−10419.

(21) Hasegawa, J.; Nakatsuji, H. *J. Phy. Chem. B.* **1998**, *102*, 10420−10430.

(22) Warshel, A.; Parson, W. W. *J. Am. Chem. Soc.* **1987**, *109*, 6143−6152.

(23) Warshel, A. *J. Am. Chem. Soc.* **1987**, *109*, 6152−6163.

(24) Alden, R. G.; Johnson, E.; Nagarajan, V.; Parson, W. W.; Law, C. J.; Cogdell, R. G. *J. Phys. Chem. B* **1997**, *101*, 4667−4680.

(25) Linnanto, J.; Helenius, V. M.; Oksanen, J. A. I.; Peltola, T.; Garaud, J.-L.; Korppi-Tommola, J. E. I. *J. Phys. Chem. A* **1998**, *102*, 4337−4349.

(26) Huang, X-f.; Nakanishi, K.; Berova, N. *Chirality* **2000**, *12*, 237−255. Huang, X.-f.; Rickman, B.; Borhan, B.; Berova, N.; Nakanishi, K. *J. Am. Chem. Soc.* **1998**, *120*, 6185−6186. Matile, S.; Berova, N.; Nakanishi, K.; Fleischhauer, J.; Woody, R. W. *J. Am. Chem. Soc.* **1996**, *118*, 5198−5206. Berova, N.; Gargiulo, D.; Derguini, F.; Nakanishi, K.; Harada, N. *J. Am. Chem. Soc.* **1993**, *115*, 4769−4775. Matile, S.; Berova, N.; Nakanishi, K.; Gargiulo, D.; Derguini, F.; Nakanishi, K.; Harada, N. J. *Am. Chem. Soc.* **1993**, *115*, 4769−4775. Cai, G-l.; Bezhkova, N.; Odingo, J.; Berova, N.; Nakanishi. K. *J. Am. Chem. Soc.* **1993**, *115*, 7192−7198.

(27) Metropolis, N.; Rosenbluth, A.; Rosenbluth, M.; Teller, A.; Teller, E. *J. Chem. Phys.* **1953**, *21*, 1087−1092.

(28) Crossley, M. J.; Hambley, T. W.; Mackay, L. G.; Try, A. C.; Walton, R. *J. Chem. Soc., Chem. Commun.* **1995**, 1077−1072. Crossley, M. J.; Mackay, L. G.; Try, A. C. *J. Chem. Soc., Chem. Commun.* **1995**, 1925−1927. The X-ray analysis was performed for the palladium compound, whereas the UV−vis and CD spectra were observed for the zinc compound.

(29) Yoshida, N. Y.; Ishizuka, T.; Osuka, A.; Jeong, D. H.; Cho, H. S.; Kim, D.; Matsuzaki, Y.; Nogami, A.; Tanaka, K. *Chem.*−*Eur. J.* **2003**, *9*, 58−75.

(30) Boc−$Por^{H2,S}$−OBu^t, 2-*tert*-butoxycarbonylamino-3-[5,10,15,20-tetra(*n*-butyl)porphyrin-2-ylmetylsulfanyl]propionic acid *tert*-butyl ester, was prepared by linking the β-pyrrole position of 5,10,15,20-tetra-n-butyl porphyrin (H_2TBP) to cysteine through a thioether bond. Boc−$(Por^{Zn,S})$−OBu^t is the zinc compound of the dimer of Boc−$Por^{H2,S}$−OBu^t. Details of the syntheses are to be published elsewhere. In the MC calculation, CH_3-CO−$(Por^{Zn,S})_2$−NHMe was used instead of Boc−$(Por^{Zn,S})_2$−OMe for practical reasons. Details of the syntheses of Boc−$(Por^{Zn,S})_n$−OMe (n = 1, 2, 4, and 8) will be published elsewhere.

(31) DeVoe, H. *J. Chem. Phys.* **1964**, *41*, 393−400. DeVoe, H. *J. Chem. Phys.* **1965**, *43*, 3199−3208.

(32) Harada, N.; Nakanishi, K. *Circular Dichroic Spectroscopy - Exciton Coupling in Organic Stereochemistry*; Oxford University Press: Oxford, U.K., 1983; pp 304−405.

(33) Rosenfeld, V. L. *Z. Phys.* **1928**, *52*, 161.

(34) Bohm, D. *Quantum Theory*; Prentice Hall: New York, 1961; p 427.

(35) Won, Y.; Friesner, R. A. *J. Phys. Chem.* **1988**, *92*, 2208−2214.

(36) Hayes, J. M.; Gillie, J. K.; Tang, D.; Small, G. J. *Biochim. Biophys. Acta* **1988**, *932*, 287−305.

(37) Zucchelli, G.; Jennings, R. C.; Garlaschi, F. M.; Cinque, G.; Bassi, R.; Cremonesi, O. *Biophys. J.* **2002**, *82*, 378−390.

(38) Moscovitz, A. *Tetrahedron* **1961**, *13*, 48. Kemp, C. M.; Mason, S. F. *Tetrahedron*, **1966**, *22*, 629−635. Brown, A.; Kemp, C. M.; Mason, S. F. *J. Chem. Soc.* **1971**, 751−755. Harada, N.; Kohori, J.; Uda, H.; Nakanishi, K.; Takeda, R. *J. Am. Chem. Soc.* **1985**, *107*, 423−428. Harada, N.; Takuma, Y.; Uda, H. *J. Am. Chem. Soc.* **1978**, *100*, 4029−4036. Harada, N.; Chen, S. M. L.; Nakanishi, K. *J. Am. Chem. Soc.* **1975**, *97*, 5345−5352. Harada, N.; Nakanishi, K. *Acc. Chem. Res.* **1972**, *5*, 257−263.

(39) Koolhaas, M. H. C.; van der Zwan, G.; Frees, R. N.; van Grondelle, R. *J. Phys. Chem.* **1997**, *101*, 7262−7270. Koolhaas, M. H. C.; Freese, R. N.; Fowler, G. J. S.; Bibby, T. S.; Georgakopoulou, S.; van der Zwaan, G.; Hunter, C. N.; van Grondelle, R. *Biochem.* **1998**, *37*, 4693−4698. Koolhaas, M. H. C.; van der Zwaan, G.; van Grondelle, R. *J. Phy. Chem., B.* **2000**, *104*, 4489−4502.

(40) Voigt function is valid on the assumption that dye integrates have symmetrical line shapes. Pitha, J.; Jones, R. N. *Can. J. Chem.* **1966**, *44*, 3031−3050.

(41) Metropolis, N.; Rosenbluth, A.; Rosenbluth, M.; Teller, A.; Teller, E. *J. Chem. Phys.* **1953**, *21*, 1087−1092.
(42) Levitt, M. *J. Mol. Biol.* **1983**, *170*, 723−764. Brünger, A. T.; Clore, G. M.; Gronenborn, A. M.; Karplus, M. *Proc. Nat. Acad. Sci. U.S.A.* **1986**, *83*, 3801−3805. Brünger, A. T.; Kuriyan, J.; Karplus, M. *Science* **1987**, *235*, 458−460. Case, D.A.; Cheatham, T.; Darden, T.; Gohlke, H.; Luo, R.; Merz, Jr. K. M.; Onufriev, A.; Simmerling, C.; Wang, B.; Woods, R. *J. Computat. Chem.* **2005**, 26, 1668−1688. Brünger, A. T. XPLOR 3.1 ed. Yale University Press: New Haven, CT, 1998.
(43) Milliè, P.; Momicchioli, F.; Vanossi, D. *J. Chem. Phys. B* **2000**, *104*, 9621−9629.
(44) Chowdhury, A.; Yu, L-P.; Raheem, I.; Peteanu, L.; Liu, L. A.; Yaron, D. J. *J. Phys. Chem. A* **2003**, *107*, 3351−3362.
(45) Hayashi, M.; Shiu, Y. J.; Chang, C. H.; Liang, K. K.; Chang, R.; Yang, T. S.; Islampour, R.; Yu, J.; Lin, S. H. *J. Chin. Chem. Soc. (Taipei*) **1999**, *46*, 381−393.
(46) Beenken, W. J. D.; Dahlbom, M.; Kjellberg, P.; Pullerits, T. *J. Chem. Phys.* **2002**, *117*, 5810−5820.
(47) Cornell, W. D.; Cieplak, P.; Bayly, C. I.; Gould, I. R.; Merz, Jr., K. M.; Ferguson, D. M.; Spellmeyer, D. C.; Fox, T.; Caldwell, J. W.; Kollman, P. A. *J. Am. Chem. Soc.* **1995**, *117*, 5179−5197.
(48) AMBER6: Fox, T.; Kollman, P. A. *J. Phys. Chem. B* **1998**, *102*, 8070−8079. Parm94 of AMBER 6 was used as the force field of the main chain of Boc−$(Por^{Zn,S})_2$−OBu^t (Figure 1). Force field of porphyrin moiety was prepared by a semiempirical molecular orbital method; that is, atomic charges of the porphyrin were calculated as ESP charges[49] using the PM3 Hamiltonian (MOPAC6.0),[50] from which RESP charges[51] were derived. We replaced the parameters for torsion angles and van der Waals interactions with those of similar groups and atoms in Parm94.
(49) Bersler, B. H.; Merz, K. M., Jr.; Kollman, P. A. *J. Comput. Chem.* **1990**, *11*, 431−439.
(50) Stewart, J. J. P. *QCPE Bull.* **1989**; reserved as Version 6.01 by Nishida, K. of Fujitsu Co., Ltd.
(51) Bayly, C. I.; Wendy, P. C.; Cornell, W. D.; Kollman, P. A. *J. Phys. Chem.* **1993**, *97*, 10269−10280.
(52) The first term represents the torsion energy, where V_n is the depth of the well of distortion, n is the periodicity of rotation, η is the dihedral angle (given later as ϕ', ψ', and χ_{1-4}), and γ is the phase of rotation. The second and third terms represent the van der Waals and Coulombic interactions, respectively. R_{ij} in the second term represents the distance between atoms i and j. A_{ij} and B_{ij} are the Lennard-Jones parameters for repulsion and attraction, respectively, between atoms *i* and *j*. ϵ in the third term is the dielectric constant. q_i and q_j are the charges on atoms i and j. The last term is the constraints given by eq 1.
(53) Caution. ϕ' and ψ' are different from the Euler angles ϕ and ψ.
(54) Momany, F. A.; McGuire, R. F.; Burgess, A. W.; Scheraga, H. A. *J. Phys. Chem.* **1975**, *79*, 2361−2381. ECEPP: Empirical Conformational Energy Program for Peptides. Quantum Chemistry Program Exchange No. 454.
(55) For consistency between GENER and AMBER, we developed an interface subroutine. Details will be published elsewhere.
(56) Monte-Carlo program was not available for Tröger's base porphyrin and the meso−meso-linked porphyrin because the program uses dihedral angles as variables; thus, it is only applicable to peptide-bonded porphyrin arrays.
(57) It should be pointed out that, the X-ray crystallographic structure of Tröger's base porphyrin is not for the Zn compound but for the Pd compound.
(58) X-ray crystallography was carried out for the Pd compound, and AB and CD spectra were measured for the Zn compound.[28.]
(59) Optimization for Boc−$(Por^{Zn,S})_2$−OMe gave two structures with different E_{AMBER} values: −138 and −135 kcal/mol. These are different in the direction of two porphyrin side chains in relation to the peptide main chain; however, the porphyrin configurations were almost same. We practically succeeded in isolating these two structural isomers by using HPLC. Details will be published elsewhere.
(60) When θ approaches 0 or 180°, ϕ and ψ come to have a common rotational axis (gimbal lock). At this point, it is substantially difficult to attain convergence.
(61) Jelley, E. E. *Nature (London)* **1936**, *138*, 1009. Scheibe, G. *Angew. Chem.* **1936**, *49*, 563. Fleisher, E. B.; Palmer, J. M.; Srivastava, T. S.; Chatterjee, A. *J. Am. Chem. Soc.* **1971**, *93*, 3162−3167. Pasternack, R. F.; Huber, P. R.; Boyd, P.; Engasser, G.; Francesconi, L.; Gibbs, E.; Fasella, P.; Venturo, G. C.; Hinds, L. de C. *J. Am. Chem. Soc.* **1972**, *94*, 4511−4517.
(62) Czikklely, V.; Forsterling, H. D.; Kuhn, H. *Chem. Phys. Lett.*, **1970**, *6*, 207−210. Nuesch, F.; Grätzel, M. *Chem. Phys.* **1995**, *193*, 1−17. Pasternack, R. F.; Collings, P. J. *Science* **1995**, *269*, 935−939. Maiti, N. C.; Mazumdar, S.; Periasamy, N. *J. Phys. Chem.* **1998**, *102*, 1528−1538.
(63) Gouterman, M. *J. Mol. Spectrosc.*, **1961**, *6*, 138−163. Gouterman, M.; Wagnière, G. H.; Snyder, L. C. *J. Mol. Spectrosc.* **1963**, *11*, 108−127.
(64) For example, the accuracy may be given by

$$\frac{1}{nR_{AB}R_{CD}}\sum_i \frac{\sqrt{D^iR^i}}{\sigma_i^2}\max\{\Delta E^i\} \qquad (11)$$

(65) Vulto, S. I. E.; de Baat, M. A.; Louwe, R. J. W.; Permentier, H. P; Neef, T.; Miller, M.; van Amerongen, H.; Aartsma, T. J. *J. Phys. Chem. B.* **1998**, *102*, 9577−9582. Wendling, M.; Przyjalgowski, M. A.; Gülen, D.; Vulto, S. I. E.; Aartsma, T. J.; van Grondelle, R.; van Amerongen, H. *Photosynth. Res.* **2002**, *71*, 99−123. Georgakopoulou, S.; Frese, R. N.; Johnson, E.; Koolhaas, C.; Cogdell, R. J. van Grondelle, R.; van der Zwan, G. *Biophys. J.* **2002**, *82*, 2184−2197.
(66) An extremely large line width was not adopted. This simulation for Tröger's base porphyrin revealed the existence of a small but broad band at the low-energy foot of the main peak. This band is small in dipolar strength but large in optical rotatory strength (band 3 in Table 2).
(67) Conditions of AMBER calculation: MD calculations for Tröger's base porphyrin and Boc−$(Por^{Zn,S})_2$−OBu^t were performed on the NVT ensemble in $CHCl_3$ up to 500 ps with a step size of 1 fs. The distance-dependent dielectric constant $\epsilon_{ij} = r_{ij}$ and cut-off length 12 Å were used. Initial velocities of particles were set to give the Maxwell distribution of 298.15 K. Temperature was maintained by the hypothetical thermal exchange between the zinc oligomers and the heat bath. (Berendsen, H. J. C.; Postma, J. P. M.; van Gunsteren, W. F.; Dinola, A.; Haak, J. R. *J. Chem. Phys.* **1984**, *81*, 3684.) The time constant for heat bath coupling was set at 0.1 ps. Translation and rotation of the solute were removed every 250 steps. The averaged structures for the final 10 ps were used in the discussion.
(68) McLachlan, A. D.; Ball, M. A. *Mol. Phys.* **1964**, *8*, 581−595.
(69) Witkowski, A.; Moffitt, W. *J. Chem. Phys.* **1960**, *33*, 872−875. Merrifield, R. E. *J. Chem. Phys.* **1964**, *40*, 445−450.
(70) Georgakopoulou, S.; Frese, R. N.; Johnson, E.; Koolhaas, C.; Cogdell, R. J.; van Grondelle, R.; van der Zwan, G. *Biophys. J.* **2002**, *82*, 2184−2197.
(71) Meyers, A. I.; Nguyen, T.; Stoianova, D.; Sreerama, N.; Woody, R. W.; Koslowski, A.; Fleischhauer, J. *Chirality* **1997**, *9*, 431−434.
(72) Medforth, C. J.; Berber, M. D.; Smith, K. M. *Tetrahedron Lett.* **1990**, *31*, 3719−3722. Song, X-Z.; Jentzen, W.; Jaquinod, L.; Khoury, R. G.; Medforth, C. J.; Jia, S.-L.; Ma, J.-G.; Smith, K. M.; Shelnutt, J. A. *Inorg. Chem.* **1998**, *37*, 2117−2128. Barkigia, K. M.; Chantraupong, L.; Smith, K. M.; Fajer, J. *J. Am. Chem. Soc.* **1988**, *110*, 7566−7567.
(73) Zewail, A. H.; Smith, D. D.; Lemaisre, J-P. *Excitons*; North-Holland Publishing Co., Amsterdam, 1982; pp 665−708.
(74) Malyshef, V. A.; Rodriguez, A.; Dominguez-Adame, F. *Phys. Rev. B.* **1999**, *60*, 14140−14146.
(75) Dominguez-Adame, F.; Malyshef, V. A. *J. Chem. Phys.* **2000**, *112*, 3023−3030.
(76) Solladié, H.; Hamel, A.; Gross, M. *Tetrahedron Lett.* **2000**, *41*, 6075−6078.
(77) The vaule k_V was derived as follows: the dipole strength *D* was calculated out from the area of the experimental absorption spectrum based on eq 12. If we use the Voigt function given by eq 13, where *h* denotes the height of the spectrum function, we obtain the integral $S \approx 1.501882 \times (h\Delta\sigma)$.

$$D^i = 9.184 \times 10^{-39}\int_0^\infty \{\epsilon(\sigma)/\sigma\}\,\mathrm{d}\sigma = (9.184 \times 10^{-39}/\sigma_{0i})\int_0^\infty \epsilon(\sigma)\,\mathrm{d}\sigma \qquad (12)$$

$$\epsilon(\sigma) = h \times \exp\left\{-\ln 2\,\frac{(\sigma-\sigma_{0i})^2}{\Delta\sigma^2}\right\}\frac{1}{1+(\sigma-\sigma_{0i})^2/\Delta\sigma^2} \qquad (13)$$